RSC Advances

PAPER

View Article Online
View Journal | View Issue

Cite this: *RSC Adv.*, 2017, **7**, 42113

Study on non-isothermal crystallization behavior of isotactic polypropylene/bacterial cellulose composites

Bo Wang,[ab] Hai-Rong Zhang,[b] Chao Huang,[b] Lian Xiong,[b] Jun Luo*[c] and Xin-de Chen*[b]

Bacterial cellulose (BC) has great potential to be used as a new filler in reinforced isotactic polypropylene (iPP) due to its characteristics of high crystallinity, biodegradability and efficient mechanical properties. But the compatibility between BC and iPP is poor. The esterification modified BC (CO) and addition of maleic anhydride grafted polypropylene (MAPP) as a compatibilizer were both used to improve interfacial compatibility of iPP and BC to prepare iPP/BC composites, and the non-isothermal crystallization behavior of isotactic polypropylene/bacterial cellulose composites was discussed. The results showed that with the addition of CO or MAPP, the compatibility of iPP/BC composites greatly improved. Moreover, BC addition was found to enhance iPP crystallization due to homogeneous and heterogeneous nucleation effects. In non-isothermal crystallization kinetics, it was found that the Jeziorny method and $\phi-t$ analysis are more accurate to describe non-isothermal crystallization behavior of iPP/BC composites. The results showed that the non-isothermal crystallization rates increase in the order of iPP/BC2, iPP, iPP/CO2, and M-iPP/BC3, indicating that the compatibility of iPP/BC composites. Moreover, the cooling rate have greatly influence on non-isothermal crystallization behavior of iPP/BC composites.

Received 14th July 2017
Accepted 12th August 2017

DOI: 10.1039/c7ra07731a

rsc.li/rsc-advances

1. Introduction

Isotactic polypropylene (iPP) is a kind of general purpose resin widely used in packaging, construction and other industrial applications.[1] It has many excellent properties such as relatively low cost, low density, and chemical resistance. However, its poor impact properties, especially at low temperature, limit its extensive use in industries.[2–4]

In order to broaden the scope of application of iPP, many modifications have been proposed, such as physical modification (blending modification) and chemical modification.[5] Among them, blending modification has advantages such as convenient operation and good modification effect and is economical.[6,7]

Bacterial cellulose (BC) is a kind of synthetic biodegradable polymer which was widely used in materials, food, and medicine.[8] BC has a superfine fiber network and has many advantageous properties such as high purity, high crystallinity, high Young's modulus, and good mechanical properties.[9] Based on these advantages, BC has great application value as a filler for reinforced iPP. But the incompatibility between polar BC and non-polar iPP affects the dispersion of BC in iPP and overall homogeneity of the composite structure. In our previous research, esterification-modified BC (CO) and maleic anhydride grafted polypropylene (MAPP) as a compatibilizer have both been used to improve interfacial compatibility of iPP and BC.[4,10] The results show that BC enhances mechanical properties of iPP and the effect of MAPP addition is better than that of esterification-modified BC.

As is known, mechanical properties of crystalline polymers are closely related to their crystallization behavior.[11–14] Generally, the study of crystallization of polymers is an idealized isothermal condition, which greatly simplifies mathematical analysis but fails to explain different cooling rates and temperatures typically encountered within the polymer in application. However, the study of crystallization in a variable-temperature environment is more practical because industrial processes generally occur under non-isothermal conditions.[15] At present, extensive research has been conducted on non-isothermal crystallization kinetics of iPP composites.[16,17] Basically, isothermal crystallization is taken as a starting point, and a partial correction is then made according to the characteristics of non-isothermal crystallization in the DSC data. The

[a]*School of Chemistry and Chemical Engineering, Taiyuan University of Science and Technology, Taiyuan, Shanxi 030024, China*

[b]*Key Laboratory of Renewable Energy, Guangzhou Institute of Energy Conversion, Chinese Academy of Sciences, Guangzhou 510640, China. E-mail: cxd_cxd@hotmail.com*

[c]*Guangzhou Fibre Product Testing and Research Institute, Guangzhou 510220, China. E-mail: luoj@gtt.net.cn*

commonly used methods include the Jeziorny method,[18] the Ozawa method,[19] and ϕ–t analysis.[20]

In this study, iPP/BC composites were prepared using a twin-screw extruder. FT-IR and SEM measurements were used for compatibility analysis of iPP/BC. The Jeziorny method, Ozawa method, and ϕ–t analysis were incorporated and compared in order to study the non-isothermal crystallization kinetics of iPP/BC composites from differential scanning calorimetry (DSC) measurements. Melting behavior after non-isothermal crystallization process was also discussed.

2. Materials and methods

2.1 Feedstock sources

iPP (S1003), with a melt flow index (MFI) of 3.6 g/10 min, $M_w = 3.2 \times 10^5$ was supplied by Sinopec Beijing Yanshan Company (China). MAPP (CMG9801), 1% grafting was purchased from Nantong Sunny Polymer New Material Technology Co., Ltd (China). A BC film (Hainan Yida Food Industry Co., Ltd. China) was flushed with deionized water till neutral, freeze-dried, and then milled into a powder (20–200 nm). Pyridine and caprylyl chloride were purchased from Aladdin Industrial Corporation, Shanghai, China.

2.2 Preparation of CO

First, the BC powder and pyridine (w/w, 1 : 20) were dispersed in a flask with a stir bar at room temperature for 30 min, and the temperature of the system was then increased to 80 °C. When the temperature of the system stabilized, the caprylyl chloride (with a mass ratio of BC 30 : 1) was added dropwise through a dropping funnel. After 7 h, the solid product of the system was washed with ethyl alcohol and deionized water to neutralize the product and dried in an air-oven for 12 h to obtain CO. Under this condition, the esterification degree of CO was 2.32.[4]

2.3 Preparation of iPP/BC composites

The mixing weight ratio of the composites is shown in Table 1. Each component was mixed in a high-speed mixer (SHR-5A, Laizhou Shenglong Chemical Machinery CO., Ltd., China) for 5 min at a speed of 2000 rpm. The pellets of the composites were prepared using a twin-screw extruder (SHJ-20, Nanjing Jieya Extrusion Equipment CO., Ltd., China). The temperatures of divisions were set to 170, 185, 195, and 200 °C. At last, the pellets were dried at 80 °C for 12 h and iPP/BC composites were obtained.

Table 1 Formula of iPP/BC composites

Sample	iPP (g)	BC (g)	CO (g)	MAPP (g)
iPP	1000	—	—	—
iPP/BC2	1000	20	—	—
iPP/CO2	1000	—	20	—
M-iPP/BC3	1000	30	—	70

2.4 Characterization of iPP/BC composites

Thermal analysis was carried out on a DSC (Q2000, TA Company, USA). The temperature and heat capacity were calibrated by pure indium standard material. For non-isothermal crystallization, the samples were first heated to 220 °C at a rate of 10 °C min^{-1}, maintained at 220 °C for 5 min to erase thermal history and cooled to 50 °C at three preset cooling rates of 5, 10, and 30 °C min^{-1}. Then, the samples were subsequently heated to 220 °C at 10 °C min^{-1}. The heat flows during both crystallization and melting processes were recorded for subsequent data analysis.

X-ray diffraction spectra were recorded from 2θ of 0° to 40° with an XRD diffraction instrument (Rigaku D/max-250, PANalytical Company, Netherlands), with a Cu Kα radiation source at λ of 0.154 nm (10 kV, 100 mA).

For FT-IR, the samples were pressed into slices (100 μm) by a heat press (170 °C, 12 MPa) for 3 min. FT-IR tests were performed on an infrared spectrometer (NICOLET iS50, Thermo Scientific Company, USA), taking 64 scans for each sample.

SEM photographs were obtained on a scanning electron microscope (S-4800, Hitachi, Japan) at an accelerated voltage of 10 kV in order to observe the compatibility of the composites.

3. Results and discussion

3.1 FT-IR of iPP/BC composites

FT-IR spectra of iPP/BC composites is shown in Fig. 1. All samples showed characteristic absorption peaks of iPP such as stretching, deformation and rocking vibration of –CH_3 (2953 cm^{-1}, 2873 cm^{-1}, 1377 cm^{-1}, 1156 cm^{-1} and 971 cm^{-1}) and stretching and flexural vibration of –CH_2 (2917 cm^{-1}, 2845 cm^{-1} and 1459 cm^{-1}). The O–H stretching vibration absorption peak was shown in the FT-IR spectra of iPP/BC composites. Especially, a new C=O group vibration appeared at 1743 cm^{-1} for iPP/CO2, M-iPP/BC3. The effect of BC esterification and addition of MAPP was confirmed by this absorption

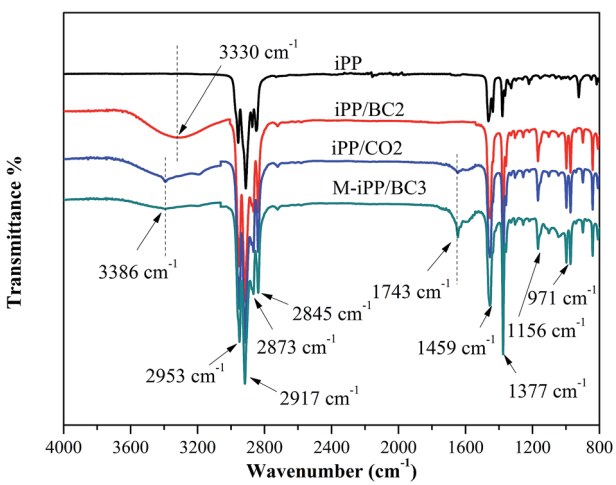

Fig. 1 FT-IR of iPP/BC composites.

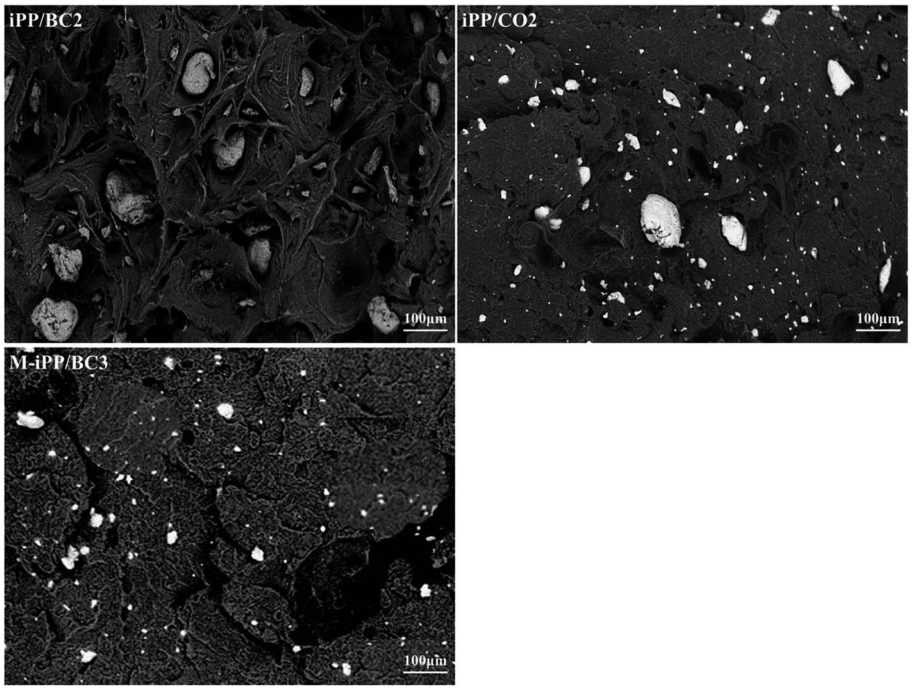

Fig. 2 SEM photographs of iPP/BC composites.

peak. Besides, compared to iPP/BC2, the O–H stretching vibration absorption peak of iPP/CO2 and M-iPP/BC3 moved to a higher wavenumber (3330–3386 cm^{-1}), peak intensity weakened, and peak width narrowed, indicating that the hydrogen bond structure of BC molecules was weakened and some hydroxyl groups were substituted after modification.[4]

3.2 SEM photographs of iPP/BC composites

SEM photographs of the composites are shown in Fig. 2. It can be seen that particle size of BC in iPP/BC2 is larger. This reflects the poor dispersion of BC in iPP. However, on BC esterification or addition of MAPP, the particle size of BC and remaining holes become smaller, thus improving compatibility. The particle size of BC in M-iPP/BC3 composites is smaller than in

Table 2 Non-isothermal crystallization parameters of iPP/BC composites

Sample	T_{on} (°C)	T_p (°C)	ΔH (J g^{-1})
iPP	122.53	119.07	97.23
iPP/BC2	123.86	119.97	95.82
iPP/CO2	122.47	120.10	96.82
M-iPP/BC3	124.19	121.08	92.65

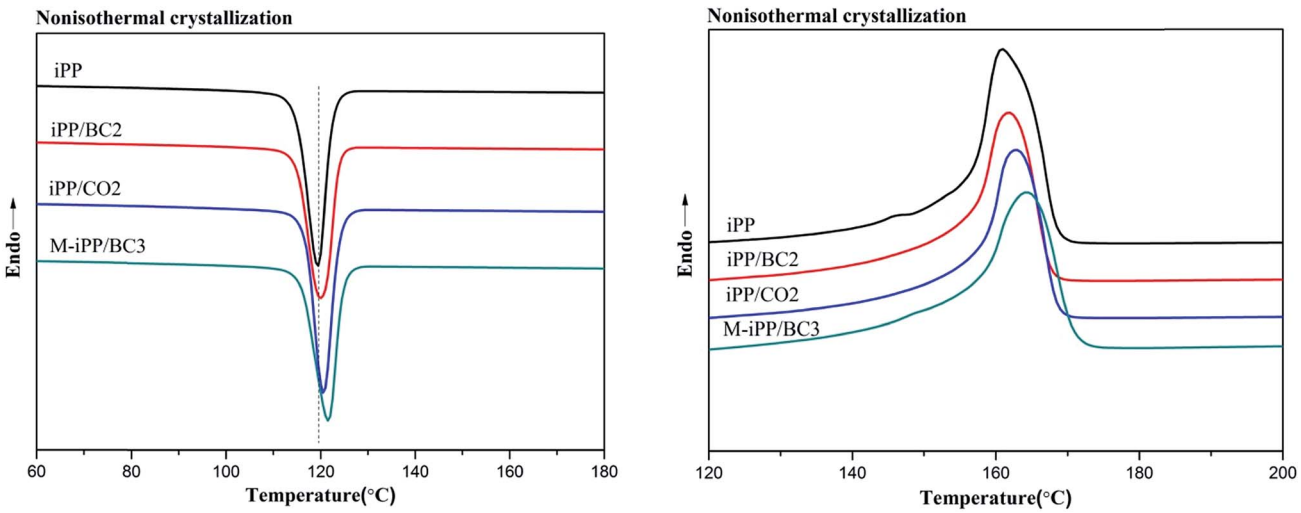

Fig. 3 Non-isothermal crystallization DSC curves of iPP/BC composites (cooling rate 10 °C min^{-1}).

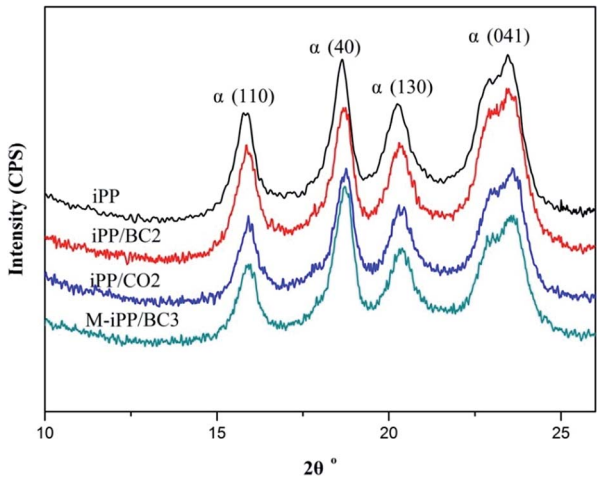

Fig. 4 XRD spectra of iPP/BC composites.

iPP/CO2. This proves that the increasing order of contribution to compatibility of the composites is iPP/BC2 iPP/CO2, and M-iPP/BC3.

3.3 Non-isothermal crystallization process of iPP/BC composites

Non-isothermal crystallization DSC curves of iPP/BC composites are shown in Fig. 3. It can be observed that BC can promote crystallization of iPP, which is demonstrated by the shift of non-isothermal crystallization curves of the sample towards higher temperatures. This indicates that the addition of BC promotes crystallization of the composites. Meanwhile, all samples have only one crystallization exothermic peak. In general, homogeneous nucleation and heterogeneous nucleation are common in crystalline polymers or their mixtures. However, iPP and BC are completely incompatible in the molten state of the system under study. Thus, we can speculate that BC-induced iPP crystallization can only be obtained by heterogeneous nucleation.

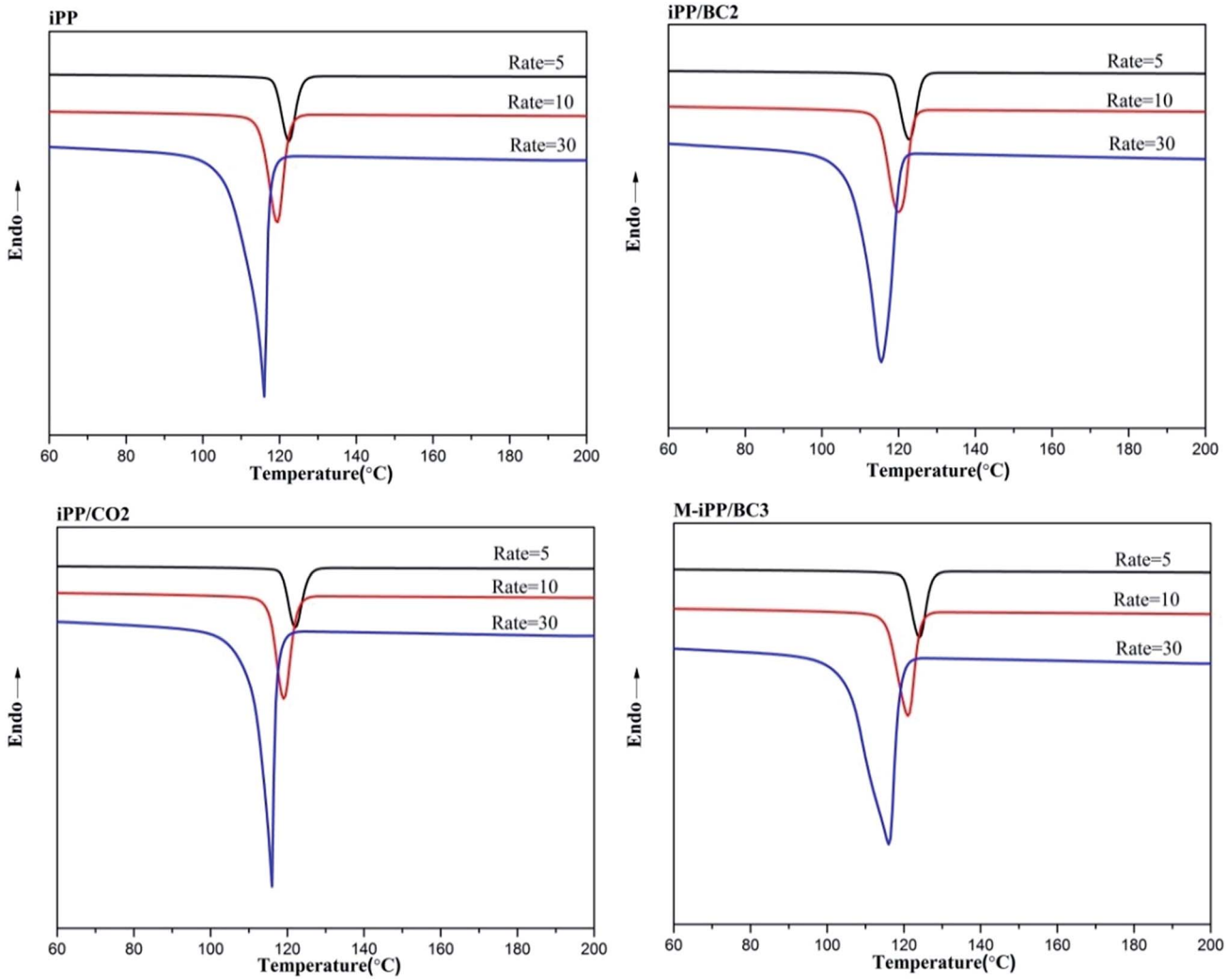

Fig. 5 Non-isothermal DSC curves of iPP/BC composites at different cooling rates.

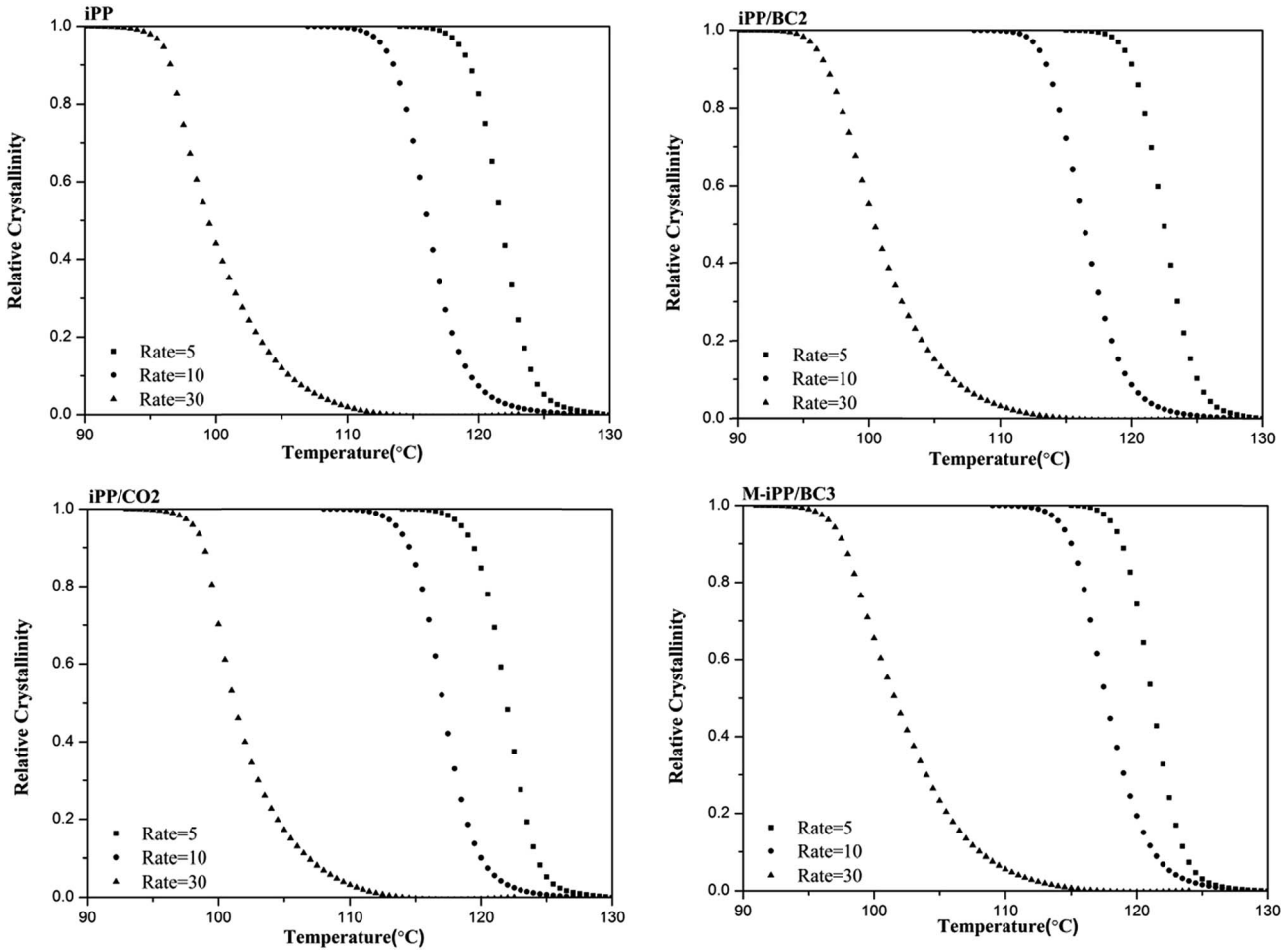

Fig. 6 Relationship between relative crystallization and crystallization temperature of iPP/BC composites during non-isothermal crystallization.

The crystallization peak parameters of composites were listed in Table 2. Compared to iPP, the peak temperature (T_p) of the iPP/BC composites increase by 0.9 °C (iPP/BC2), 0.94 °C (iPP/CO2), and 2.01 °C (M-iPP/BC3), respectively. Meanwhile, peak width slightly narrows, indicating that the addition of BC effectively shortens the induction time of iPP crystals and increases crystallization rate of the composites. The order of contribution to crystallinity of the composites is BC < CO < MAPP as the compatibilizers, which conforms to the effects of the two modification methods on the mechanical performance of the composites, as mentioned in our previous research.[4,10] In addition, the crystallinity enthalpy rates of the composites indicate that the crystallinity of the samples are not quite different, which can also be seen from Fig. 4. Moreover, it can be noted that only α-crystals can be produced by the induction of iPP regardless of the method of modification.

3.4 Non-isothermal crystallization kinetics analysis of iPP/BC composites

Non-isothermal crystallization curves at sample cooling rates of 5 °C min^{-1}, 10 °C min^{-1}, and 30 °C min^{-1} are shown in Fig. 5. It can be seen from Fig. 5 that as the cooling rate increases, crystallization temperature (T_p) decreases and the crystallization peak widens. The main reason for this phenomenon is molecular chain activity at a relatively low temperature is poor, which causes the formation of crystal imperfections. Hence, the crystal can crystallize at low temperature (T_p value decrease), the perfection of crystallization is different, and the range of melting temperatures becomes larger (crystallization peak becomes wider).

In order to further analyze non-isothermal crystallization, crystallization kinetics of iPP/BC composites were compared. Based on the assumption that the evolution of crystallinity is linearly proportional to the evolution of heat released during crystallization, the relative degree of crystallinity, $X_w(t)$, was calculated by integration of exothermal peaks from eqn (1).

$$X_w(t) = \int_{t_0}^{t} \left(\frac{dH}{dt}\right) \Big/ \int_{t_0}^{t_\infty} \left(\frac{dH}{dt}\right) dt \quad (1)$$

where dH/dt is crystallization heat flow rate at a temperature of t and t_0 and t_∞ correspond to starting and ending temperatures of crystallization, respectively. In eqn (1), $X_w(t)$ at any crystallization temperature is converted to volume fraction relative crystallinity $X(t)$, as shown in Fig. 6.

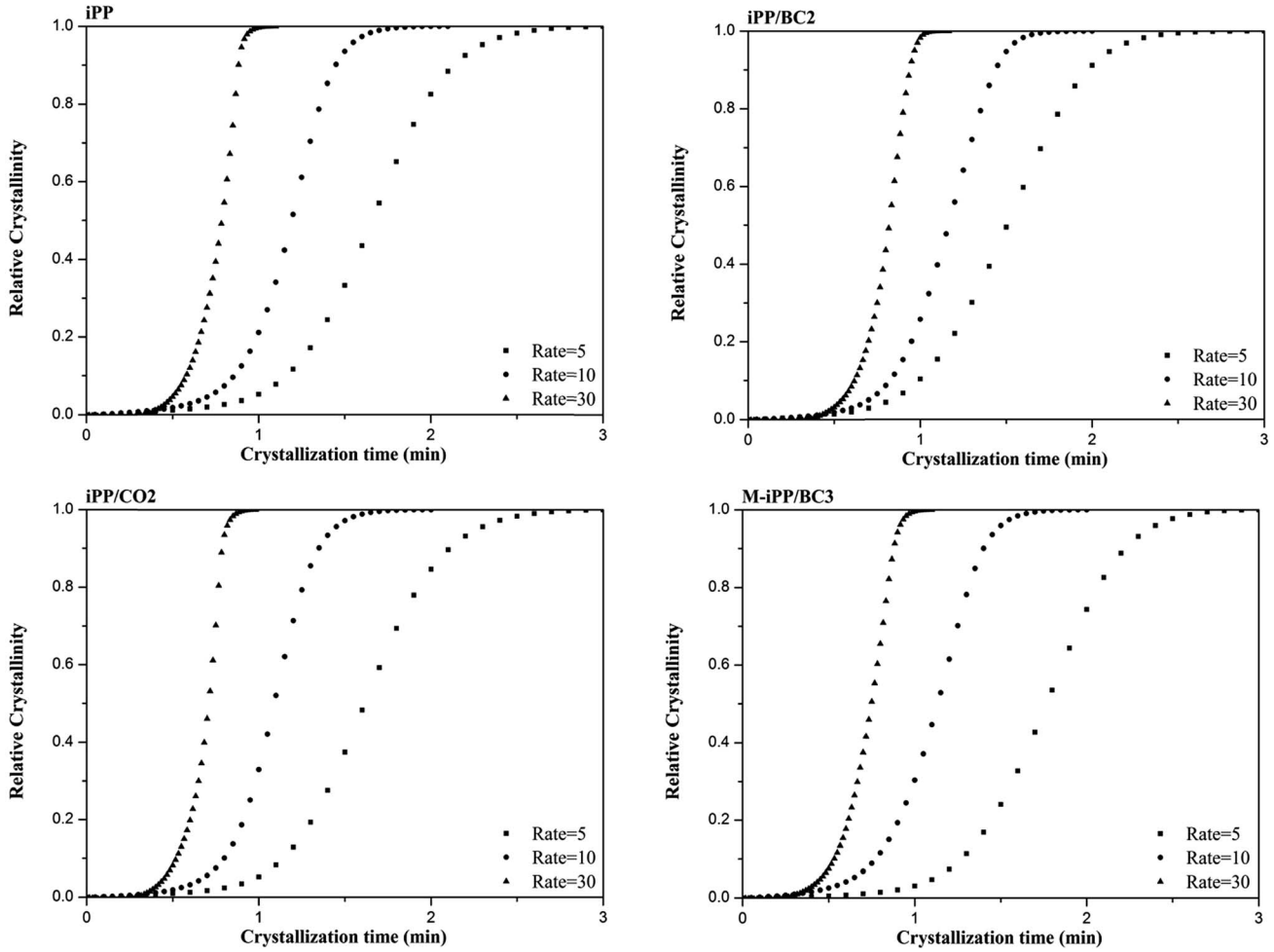

Fig. 7 Relationship between relative crystallization and crystallization time of iPP/BC composites during non-isothermal crystallization.

The relationship between crystallinity $X(t)$ and temperature T can be converted to that between crystallinity $X(t)$ and time t, as shown in Fig. 7 *via* eqn (2).

$$t = (T_0 - T)/\phi \quad (2)$$

3.4.1 Jeziorny method. The Avrami equation (eqn (3)) describes isothermal crystallization kinetics of crystalline polymers. The equation describes how solids transform from one state of matter or phase to another at constant temperature and can also describe some types of chemical reactions.[21,22]

$$X(t) = 1 - \exp(-Kt^n) \quad (3)$$

where $X(t)$ is time-dependent relative crystallinity, n is Avrami exponent, K is crystallization rate constant, and t is crystallization time. The Avrami exponent n depends on type of nucleation and growth process, and the value of n is between 1 and 4.[23]

Eqn (3) is typically rearranged in a linear form as double logarithm eqn (4):

$$\log[-\ln(1 - X(t))] = n \log t + \log K \quad (4)$$

The Jeziorny method modifies the Avrami equation to describe non-isothermal crystallization kinetics of polymers. The Jeziorny method is a direct method to apply the Avrami equation to non-isothermal crystallization. It calibrates parameters by taking non-isothermal crystallization as isothermal crystallization, so that non-isothermal crystallization mechanism of the polymer is determined.[18]

A corrected form of the rate term (K) used in the Avrami equation assuming a constant cooling/heating rate is proposed. The relative crystallinity at a set cooling rate (R) is a function of crystallization temperature (T).

The plot of $\log[-\ln(1 - X(t))]$ against $\log(t)$ is obtained based on eqn (4). The Avrami index n is obtained from the slope, and $\log K$ can be obtained from the intercept. Correction of cooling rate ϕ is made for the obtained K (eqn (5)).

$$\log K_c = (\log K)/\phi \quad (5)$$

Fig. 8 and Table 3 are obtained by processing the data in Fig. 6 using the Jeziorny method. It can be seen from Table 3 that the n values are around 3 and the n value of iPP is larger than of other samples. This indicates that the composites follow a three-dimensional growth pattern and due to the addition of

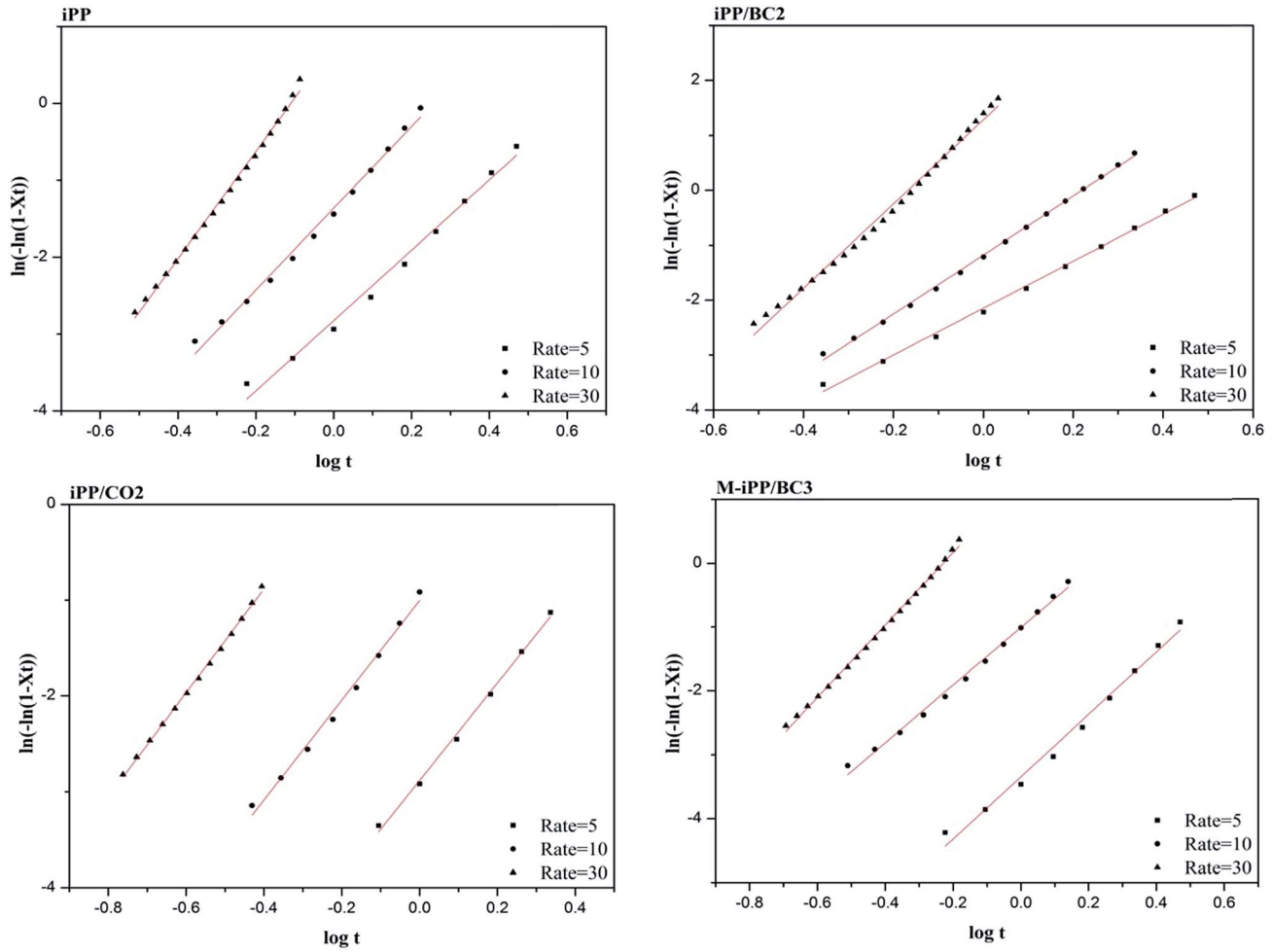

Fig. 8 Non-isothermal crystallization kinetics curves of iPP/BC composites (Jeziorny method).

BC, homogeneous nucleation and heterogeneous nucleation coexist in the composites.

Table 3 also prove that K_c value of the samples increases with cooling rate, while semi-crystallization time ($t_{1/2}$) of the sample decreases, which shows that crystallization rate of the composites is proportional to cooling rate. This is because at a low cooling rate, the transition speed from melting state to crystalline state of the composites is slow and the impact of cooling rate on crystallization is weak. At the same cooling rate, K_c values of the samples increase gradually, which indicates that BC promotes crystallization of the composites.

Table 3 Non-isothermal crystallization kinetics parameters (Jeziorny method)

Sample	ϕ	T_p (°C)	T_{on} (°C)	ΔH (J g^{-1})	n	k	$t_{1/2}$ (min)
iPP	5	122.41	125.64	96.95	3.9	0.0001	1.66
	10	119.07	122.53	97.23	3.8	0.0044	1.19
	30	116.26	116.76	97.09	3.7	0.1963	0.78
iPP/BC2	5	122.74	126.06	96.48	3.5	0.0003	1.62
	10	119.97	123.86	95.82	3.4	0.0066	1.16
	30	115.46	120.36	94.17	3.7	0.6499	0.72
iPP/CO2	5	122.06	125.48	97.38	3.6	0.0007	1.57
	10	120.10	122.47	96.82	3.7	0.0098	1.09
	30	116.24	116.53	97.46	3.4	0.6599	0.71
M-iPP/BC3	5	124.05	127.20	93.52	3.3	0.0014	1.46
	10	121.08	124.19	92.65	3.1	0.0100	1.03
	30	116.15	118.85	92.81	3.4	0.6651	0.65

3.4.2 Ozawa analysis. The Ozawa analysis is also a commonly used method for non-isothermal crystallization kinetics of polymers; its mathematical expression is as follows (eqn (6)).

$$1 - X(T) = \exp(1 - Z(T))/\phi \quad (6)$$

Logarithmic transformation of eqn (6) produces eqn (7):

$$\log[-\ln(1 - X(T))] = \log(1 - Z(T)) - m \log \phi \quad (7)$$

where m stands for Ozawa index and $Z(T)$ stands for kinetics parameter and is a function of temperature T, which is related to nucleation mode, rate, and crystal growth mode of the polymer. If the system conforms to the Ozawa equation, a curve should be obtained by plotting $\log \phi$ against $\log [-\ln(1 - X(T))]$ in eqn (7) at a certain temperature. The slope of the straight line equals the Ozawa index m and the intercept equals the kinetics parameter $Z(T)$.

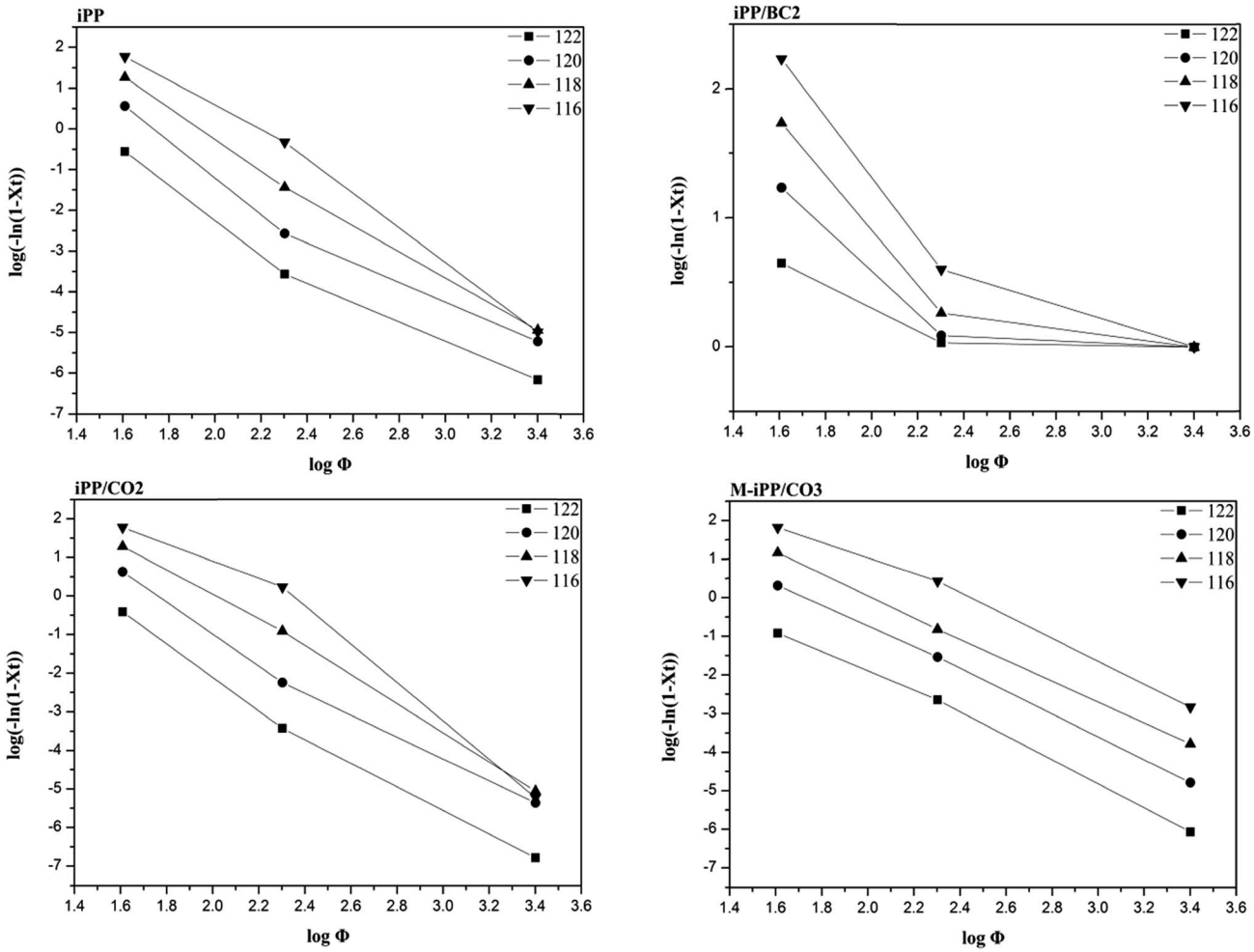

Fig. 9 Non-isothermal crystallization kinetics curves of iPP/BC composites (Ozawa method).

The non-isothermal data of each sample were processed using Ozawa analysis, and the results obtained are shown in Fig. 9 and Table 4. It can be seen that non-isothermal crystallization kinetics curves are linear for iPP, iPP/CO2, and M-iPP/BC3, but not for iPP/BC2. The $Z(T)$ value of the sample shows a tendency to decrease as temperature increases, except iPP/BC2. The $Z(T)$ value of the modified sample are higher than of pure iPP, which also indicates that the interfacial compatibility of the material is improving and thus its crystallinity. However, regularity has not been shown in the $Z(T)$ value of the iPP/BC2 sample, which indicates that poor interface compatibility affects nucleation and growth of the composites.

Table 4 Non-isothermal crystallization kinetics parameters (Owaza method)

	iPP		iPP/BC2		iPP/CO2		M-iPP/B3	
T (°C)	m	$Z(T)$	M	$Z(T)$	m	$Z(T)$	m	$Z(T)$
116	−3.16	3.82	−1.18	5.28	−4.00	6.21	−2.63	8.69
118	−3.06	2.87	−0.90	4.04	−3.56	5.57	−2.76	7.11
120	−3.82	1.99	−0.64	8.13	−3.30	5.01	−2.86	5.72
122	−3.44	1.04	−0.33	6.68	−3.51	3.84	−2.89	4.96

3.4.3 ϕ–t analysis. Another treatment for non-isothermal crystallization is the ϕ–t analysis. The relationship between crystallization time t and cooling rate ϕ is established by ϕ–t analysis (eqn (8)).

$$\log \phi = \log F(T) - a \log t \tag{8}$$

where $F(T) = [Z(T)/k]^{1/m}$ represents cooling rate required to reach a certain crystallinity in unit crystallization time and a denotes ratio of Avrami index to Ozawa index.

Using ϕ–t analysis, non-isothermal crystallization kinetics curves of each sample are obtained by plotting $\log \phi$ against $\log t$, as shown in Fig. 10. It can be seen that $\log \phi$ of each sample analyzed by the ϕ–t method shows a good linear relationship with $\log t$. The kinetics parameters a and $F(T)$ are obtained using the slope and intercept of the straight line, as shown in Table 5.

As shown in Table 5, the $F(T)$ and a values of the samples increase with crystallinity. This indicates that crystallinity of the composites can be increased by accelerating the cooling rate and the degree of crystal refinement increases as crystallization progresses.

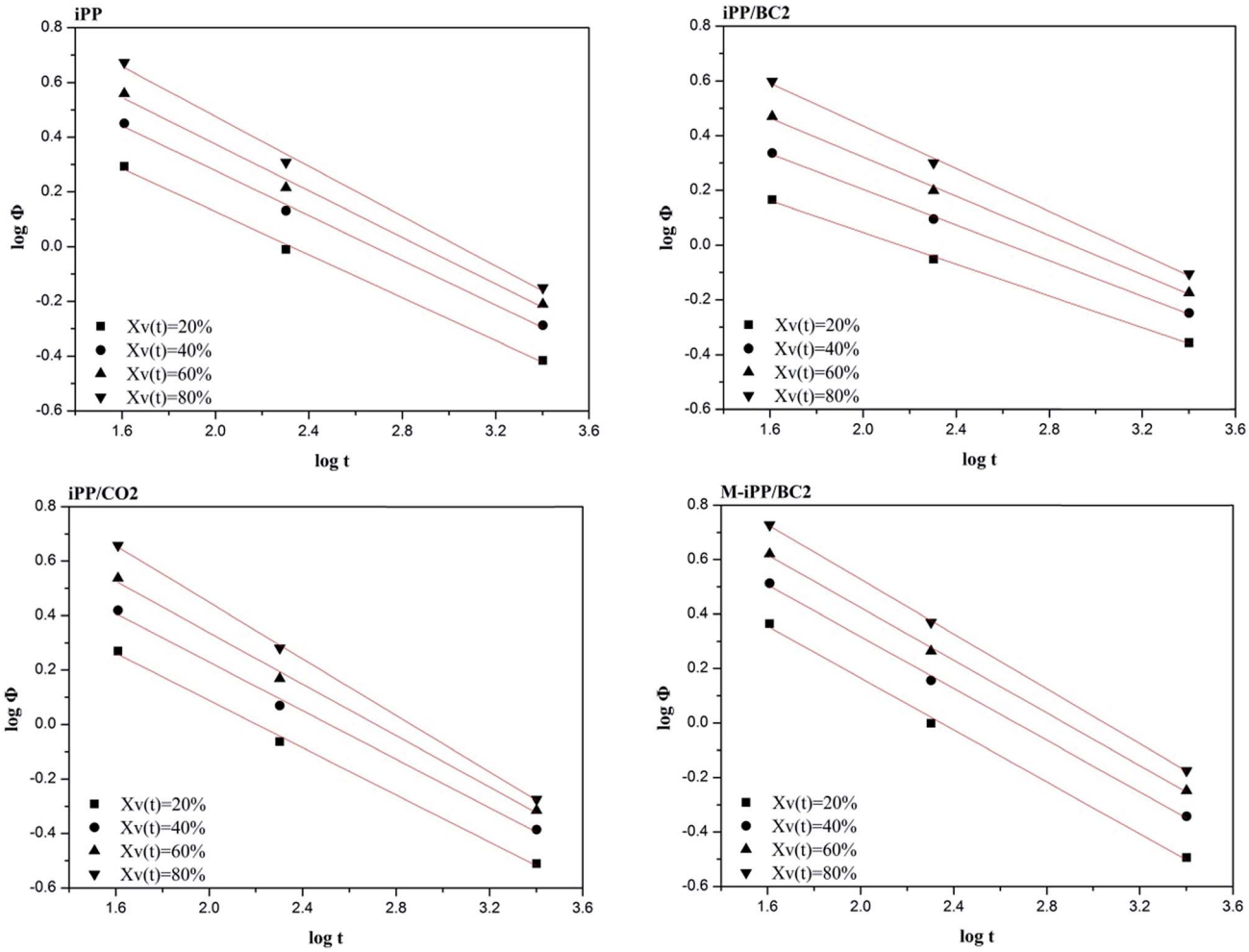

Fig. 10 Non-isothermal crystallization kinetics curve of iPP/BC composites (ϕ–t analysis).

However, the a values of samples for same crystallinity in ascending order are iPP/BC2, iPP, iPP/CO2, and M-iPP/BC3, and the a value of iPP/BC2 is lower than that of the others at the same crystallinity, showing that the poor compatibility of the iPP/BC2 sample leads to a lowered crystallization rate.

Table 5 Non-isothermal crystallization kinetics parameters (ϕ–t analysis)

Sample	$X(t)$ (%)	$F(T)$	a
iPP	20	0.91	0.39
	40	1.10	0.41
	60	1.23	0.43
	80	1.39	0.46
iPP/BC2	20	0.63	0.29
	40	0.85	0.32
	60	1.04	0.36
	80	1.22	0.39
iPP/CO2	20	0.95	0.43
	40	1.12	0.45
	60	1.28	0.47
	80	1.49	0.52
M-iPP/BC3	20	1.12	0.48
	40	1.27	0.48
	60	1.39	0.48
	80	1.53	0.50

4. Conclusion

iPP/BC composites were successfully prepared using a twin-screw extruder. The compatibility and crystallization behavior of the composites was studied by FT-IR, SEM, XRD and DSC. With BC esterification or MAPP addition, compatibility of iPP/BC composites was greatly improved. The addition of BC was found to enhance crystallization of iPP due to homogeneous and heterogeneous nucleation effects. In non-isothermal crystallization kinetics, it was found that the Jeziorny method and ϕ–t analysis were more accurate to describe non-isothermal crystallization behavior of iPP/BC composites. The result of non-isothermal crystallization kinetics analysis of the composites showed that non-isothermal crystallization rates increase in the order of iPP/BC2, iPP, iPP/CO2, and M-iPP/BC3, indicating that the compatibility of iPP/BC composites and the cooling rate have considerable influence on non-isothermal crystallization behavior of iPP/BC composites.

Conflicts of interest

There are no conflicts to declare.

Acknowledgements

The authors acknowledge the financial support of the CAS Key Laboratory of Renewable Energy (No. Y707k91001), the Doctoral Startup Project of Taiyuan University of Science and Technology (20162013) and the National Natural Science Foundation of China (51303181).

References

1 M. Kontopoulou, W. Wang, T. Gopakumar and C. Cheung, *Polymer*, 2003, **44**, 7495–7504.
2 Y. Pang, X. Dong, Y. Zhao, C. C. Han and D. Wang, *Polymer*, 2007, **48**, 6395–6403.
3 W. Weng, W. Hu, A. H. Dekmezian and C. J. Ruff, *Macromolecules*, 2002, **35**, 3838–3843.
4 B. Wang, D. Yang, H. R. Zhang, C. Huang, L. Xiong, J. Luo and X. D. Chen, *Polymers*, 2016, **8**, 129.
5 C. Giavarini, P. D. Filippis, M. L. Santarelli and M. Scarsella, *Fuel*, 1996, **75**, 681–686.
6 W. Qiu, T. Endo and T. Hirotsu, *J. Appl. Polym. Sci.*, 2006, **102**, 3830–3841.
7 T. Semba, K. Kitagawa, M. Nakagawa, U. S. Ishiaku and H. Hamada, *J. Appl. Polym. Sci.*, 2005, **98**, 500–508.
8 C. Huang, X. Y. Yang, L. Xiong, H. J. Guo, J. Luo, B. Wang, H. R. Zhang, X. Q. Lin and X. D. Chen, *Appl. Biochem. Biotechnol.*, 2015, **175**, 1678–1688.
9 C. R. Clark, N. Baril, M. Kunicki, N. Johnson, J. Soukup, K. Ferguson, S. Lipsitz and J. Bigby, *Cellulose*, 2009, **16**, 1033–1045.
10 B. Wang, H. R. Zhang, C. Huang, L. Xiong, J. Luo and X. D. Chen, *Polymer*, 2017, **41**, 460–464.
11 A. Salazar, A. Rico, S. Rodríguez, J. M. Navarro and J. Rodríguez, *Polym. Eng. Sci.*, 2012, **52**, 805–813.
12 B. Suksut and C. Deeprasertkul, *J. Polym. Environ.*, 2011, **19**, 288–296.
13 A. Misra and S. N. Garg, *J. Polym. Sci., Part B: Polym. Phys.*, 1986, **24**, 999–1008.
14 R. Hemanth, B. Suresha and M. Sekar, *J. Compos. Mater.*, 2015, **49**, 2217–2229.
15 M. L. D. Lorenzo and C. Silvestre, *Prog. Polym. Sci.*, 1999, **24**, 917–950.
16 A. I. Isayev and B. F. Catignani, *Polym. Eng. Sci.*, 1997, **37**, 1526–1539.
17 P. Supaphol and J. E. Spruiell, *Polymer*, 2001, **42**, 699–712.
18 A. Jeziorny, *Polymer*, 1978, **19**, 1142–1144.
19 T. Ozawa, *Polymer*, 1971, **12**, 150–158.
20 T. Liu, Z. Mo, S. Wang and H. Zhang, *Polym. Eng. Sci.*, 1997, **37**, 568–575.
21 K. M. Seven, J. M. Cogen and J. F. Gilchrist, *Polym. Eng. Sci.*, 2016, **56**, 541–554.
22 M. Joshi and B. S. Butola, *J. Appl. Polym. Sci.*, 2010, **105**, 978–985.
23 M. Avrami, *J. Chem. Phys.*, 1939, **7**, 1103–1112.